Spectroscopy 22 (2008) 123–141
DOI 10.3233/SPE-2008-0330
IOS Press

The proximal and distal pockets of the H93G myoglobin cavity mutant bind identical ligands with different affinities: Quantitative analysis of imidazole and pyridine binding

Jing Du [a], Masanori Sono [a] and John H. Dawson [a,b,*]
[a] *Department of Chemistry and Biochemistry, University of South Carolina, Columbia, SC, USA*
[b] *School of Medicine, University of South Carolina, Columbia, SC, USA*

Abstract. His93Gly sperm whale myoglobin (H93G Mb) has the proximal histidine ligand removed to create a cavity for exogenous ligand binding, making it a versatile template for the preparation of model heme complexes. In this study, we have measured the first and second ligand binding affinities of imidazole and pyridine to form mono- and bis-ligated ferric and ferrous H93G Mb complexes. Electronic absorption spectroscopy has been utilized to determine the binding affinities for the proximal (K_{d1}, first ligand) and distal (K_{d2}, second ligand) pockets of H93G Mb. Magnetic circular dichroism spectroscopy has been used to confirm the identity of the complexes. The binding affinities for the first ligand are one hundred- to one thousand-fold higher than those for the second ligand ($K_{d1} \ll K_{d2}$) for the same exogenous ligand. This is entirely opposite to what is seen with free heme in organic solvents where $K_{d1} \gg K_{d2}$. Thus, the proximal pocket is the high affinity binding site. The lower affinity for the distal pocket can be attributed to steric hindrance from the distal histidine. This report provides quantitative evidence for differential ligand binding affinities of the proximal and distal pockets of H93G Mb, a unique property that facilitates generation of heme iron derivatives not easily prepared with other heme model systems.

Keywords: H93G myoglobin, cavity mutant, proximal pocket, distal pocket, imidazole binding, pyridine binding

1. Introduction

Biological functions of heme-containing proteins are largely dependent on the iron oxidation state, heme iron coordination structure and surrounding protein environment [1]. The desire to explore the structure and mechanism of diverse heme-containing proteins has led researchers to prepare synthetic heme iron model systems in organic solvents to mimic the functional properties of native heme proteins, such as the dioxygen storage protein myoglobin (Mb) [2,3]. Such synthetic efforts have achieved considerable success over the past three decades [2–5]. However, it has suffered from certain limitations as well. Among the major challenges are the difficulties to generate stable six-coordinate synthetic heme iron systems with different axial ligands and complexes containing a single exogenous added ligand. Solutions to these challenges in model heme complexes in organic solvents have usually required elaborate synthetic efforts [2–5]. Water-soluble heme peptides derived from cytochrome c (microperoxidases) have also been used for similar purposes [6].

*Corresponding author: John H. Dawson, Department of Chemistry and Biochemistry, 631 Sumter Street, University of South Carolina, Columbia, SC 29208, USA. Tel.: +1 803 777 7234; Fax: +1 803 777 9521; E-mail: dawson@sc.edu.

Imidazole (Im), in the form of a histidine (His), serves as a very important axial ligand in heme proteins, most notably the dioxygen binding/storage protein Mb which contains a single His ligand in its functional five-coordinate deoxyferrous state. In the non-functional ferric state, histidine and water serve as proximal and distal axial ligands, respectively [7]. To investigate the importance of heme iron coordination structure, inorganic chemists have sought to prepare synthetic heme iron-Im model mimics of myoglobin [2–6]. However, iron(III) tetraphenylporphyrin (Fe(III)TPP) only forms low spin six-coordinate Fe(III)TPP$(Im)_2$ without any detectable amount of a mono-Im complex. Coyle et al. [8] studied the equilibria of Im with Fe(III)TPP in organic solvents and estimated that the equilibrium association constant (K_a value) of the second Im binding to Fe(III)TPP(Im) was more than 48 times of that of single (first) Im binding. Therefore, the Fe(III)TPP(Im) intermediate was not observed in the equilibrium reaction [8,9]. Similarly, predominantly six-coordinate iron(II) bis-Im porphyrin model has been observed upon addition of Im to ferrous heme in organic solvents [10].

The idea and successful preparation of proximal ligand cavity mutants of heme protein systems has provided researchers with relatively easy solutions in addressing these problems, especially within sophisticated diverse protein environments. This approach was pioneered by Barrick [11] with the site-directed mutant, His93Gly sperm whale Mb (H93G Mb) where the His residue serving as the natural heme iron proximal axial ligand has been replaced with a smaller non-coordinating glycine residue. This mutation creates a cavity that can be filled with various exogenous ligands to mimic the heme coordination structure of native proteins.

The Dawson research group has extensively studied H93G Mb and has shown it to be a versatile template for the preparation of model heme complexes of defined structure [12–16]. For example, H93G Mb (imidazole) and (alkylthiolate) adducts provided mimics of native Mb [13] and cytochrome P450 [14], respectively. In order to further understand the effects of the proximal and distal pockets on the ligand binding properties of H93G Mb cavity mutant, we report herein detailed equilibrium studies of the binding of two nitrogenous donor ligands, Im and pyridine (Py), to ferric and ferrous H93G Mb using electronic absorption (EA) and magnetic circular dichroism (MCD) spectroscopy. MCD spectroscopy is a particularly useful technique because it has frequently been shown to possess of greater fingerprinting capacity than EA spectroscopy for studying the electronic structures and the heme iron coordination modes of porphyrin-containing systems [17]. The work reported herein provides quantitative evidence for differential affinities of the first and second ligand binding to the heme iron of H93G Mb cavity mutant in both ferric and ferrous oxidation states. The data further demonstrate the advantage of the H93G Mb cavity mutant for the preparation of heme model complexes, including mixed ligand ferric as well as ferrous adducts, due to the difference in ligand accessibility of the proximal and distal sides of the heme.

2. Materials and methods

2.1. Chemicals and proteins

All chemicals used in this study were obtained from Aldrich or Sigma and were used without further purification unless specified otherwise. Sperm whale H93G Mb was expressed and purified in the presence of 10 mM Im as previously described [11]. The isolated protein contains Im as its proximal ligand and exists in a mixture of ferric and oxyferrous states. Complete oxidation of the heme iron is accomplished by addition of a few crystals of potassium ferricyanide (Fluka) followed by gel-filtration column chromatography. Im can be completely removed from the proximal cavity by means of heme extraction followed by reconstitution with hemin as previously reported [18].

2.2. Ligand binding studies

H93G Mb concentrations were determined by the pyridine hemochromogen method [19]. A molar absorptivity (ε) value of 112 mM^{-1} cm^{-1} for the Soret absorption peak (405–406 nm) for exogenous ligand-free ferric H93G Mb at pH 7.0 [18] was routinely used as a reference standard value. All proximal and distal pocket ligand binding studies were carried out at pH 7.0 in 0.1 M potassium phosphate buffer at 4°C. Im stock solutions were prepared by dissolving commercial solid Im (99.9%) in 0.1 M potassium phosphate buffer and adjusting pH to 7.0 by adding HCl. Py stock solutions were prepared by diluting commercial Py (99.9%) in 0.1 M potassium phosphate buffer (pH 7.0) without pH adjustment. Ligand binding to H93G Mb was monitored by measuring changes of the electronic absorption (EA) spectrum in the Soret and visible regions using a Cary 400 spectrophotometer at 4°C. For H93G Mb, the equilibrium reaction with Im appeared to be complete in the manual mixing time (<30 s). H93G Mb concentrations used were ∼3.5 μM (1-cm cuvette) in studying first Im binding to proximal pocket and ∼35 μM (0.2-cm cuvette) in second Im binding to distal pocket, respectively. To study ligand binding to H93G Mb, pH 7 ligand stock solutions at different concentrations ranging from 2 mM to 2 M for Im and from 10 mM to 2 M for Py were used to add into a single protein solution to monitor both the first and second phases of Im or Py binding. The second phase binding was also examined in separate experiments at higher protein concentration (∼35 μM). To study ligand binding to ferrous H93G Mb, cuvettes were filled with anaerobic 0.1 M potassium phosphate buffer that had been degassed and sealed with a rubber septum. Exogenous ligand-free ferric H93G Mb was added to the buffer by using a microliter syringe. The protein solution was further degassed with a stream of nitrogen gas for 10 min, and then a few microliters of concentrated sodium dithionite solution (25 mg/ml H_2O) was added with a microliter syringe to generate ligand-free deoxyferrous H93G Mb. Measurements of ligand binding to deoxyferrous Mb were made directly on this sample by using pH 7 Im or Py stock solutions that had been made anaerobic by degassing. For each titration, ligand was added in a small increment to a single protein solution and absorbance changes were monitored to ensure that equilibrium was reached after each ligand addition.

2.3. Spectroscopic techniques

EA absorption spectra were recorded with a Cary 400 spectrophotometer interfaced to a Dell PC. MCD spectra were measured with a magnetic field strength of 1.41 T by using a JASCO J815 spectropolarimeter. This instrument was equipped with a JASCO MCD-1B electromagnet and interfaced with a Silicon Solutions PC through a JASCO IF-815-2 interface unit. All spectral measurements were performed using 0.2- or 1.0-cm cuvette at 4°C. Data acquisition and manipulation has been described previously [20]. EA spectra were recorded before and after the MCD measurements to verify sample integrity. The spectra of H93G Mb Im complexes reported in this work are in good agreement with those in previous published work [13].

2.4. Determination of dissociation constants for H93G Mb–ligand complexes

Imidazole association reactions with H93G Mb were modeled as a simple bimolecular association reaction. The equilibrium of ligand binding to H93G Mb is shown as the following simple reversible reaction (1):

$$\text{H93G Mb} + \text{L} \overset{K_\text{d}}{\leftrightarrows} \text{H93G(L) Mb}, \tag{1}$$

[H93G Mb], [H93G(L) Mb] and [L] represent the concentration of the ligand-free H93G Mb, ligand-bound H93G Mb and free ligand, respectively. By definition,

$$K_{\mathrm{d}} = [\text{H93G Mb}]\,[\text{L}]/[\text{H93G(L) Mb}]. \tag{2}$$

Fractional ligand (L) saturation (Y) of H93G Mb is defined as

$$Y = [\text{H93G(L) Mb}]/\{[\text{ H93G(L) Mb}] + [\text{H93G Mb}]\}. \tag{3}$$

Solving Eq. (2) for [H93G(L) Mb] and then substituting it into Eq. (3), we obtain

$$Y = [\text{L}]/(K_{\mathrm{d}} + [\text{L}]). \tag{4}$$

2.4.1. Hyperbolic saturation plot equation

Let ΔA be the absorbance change caused by the addition of the ligand, and $\Delta A_{\max}$ the absorbance change for the complete formation of H93G(L) Mb at infinite ligand concentration. Multiplying Eq. (4) by $\Delta A_{\max}$,

$$\Delta A = \Delta A_{\max}[\text{L}]/(K_{\mathrm{d}} + [\text{L}]). \tag{5}$$

2.4.2. Hill plot equation

Rearranging Eq. (4),

$$Y/(1 - Y) = [\text{L}]/K_{\mathrm{d}}. \tag{6}$$

By taking log of Eq. (6),

$$\log\{Y/(1 - Y)\} = \log[\text{L}] - \log K_{\mathrm{d}}. \tag{7}$$

Dissociation constants for the binding of Im to H93G were then determined by saturation hyperbolic curve fit and/or Hill plot analysis of ligand titration data.

3. Results and discussion

3.1. Electronic absorption (EA) spectra-monitored first and second ligand binding to the proximal and distal pockets of ferric H93G Mb

Exogenous ligand-free ferric H93G Mb exhibits an EA spectrum with a Soret absorption peak at 405–406 nm and charge transfer band at ~600 nm. Stepwise addition of Im to reconstituted, exogenous ligand-free ferric H93G Mb produces significant changes in the Soret and visible regions of the EA spectrum (Figs 1 and 2). There are two clear sets of isosbestic points depending on the different range of Im concentration in the protein solution during the titration. This indicates that throughout the Im binding reaction there are three optically distinct heme ligation states: exogenous ligand-free, mono-Im and bis-Im ferric H93G Mb. The EA spectral data for the first ligand binding phase (mono-Im formation) shows that micromolar addition of Im to ferric H93G Mb causes both an increase and a red-shift of the

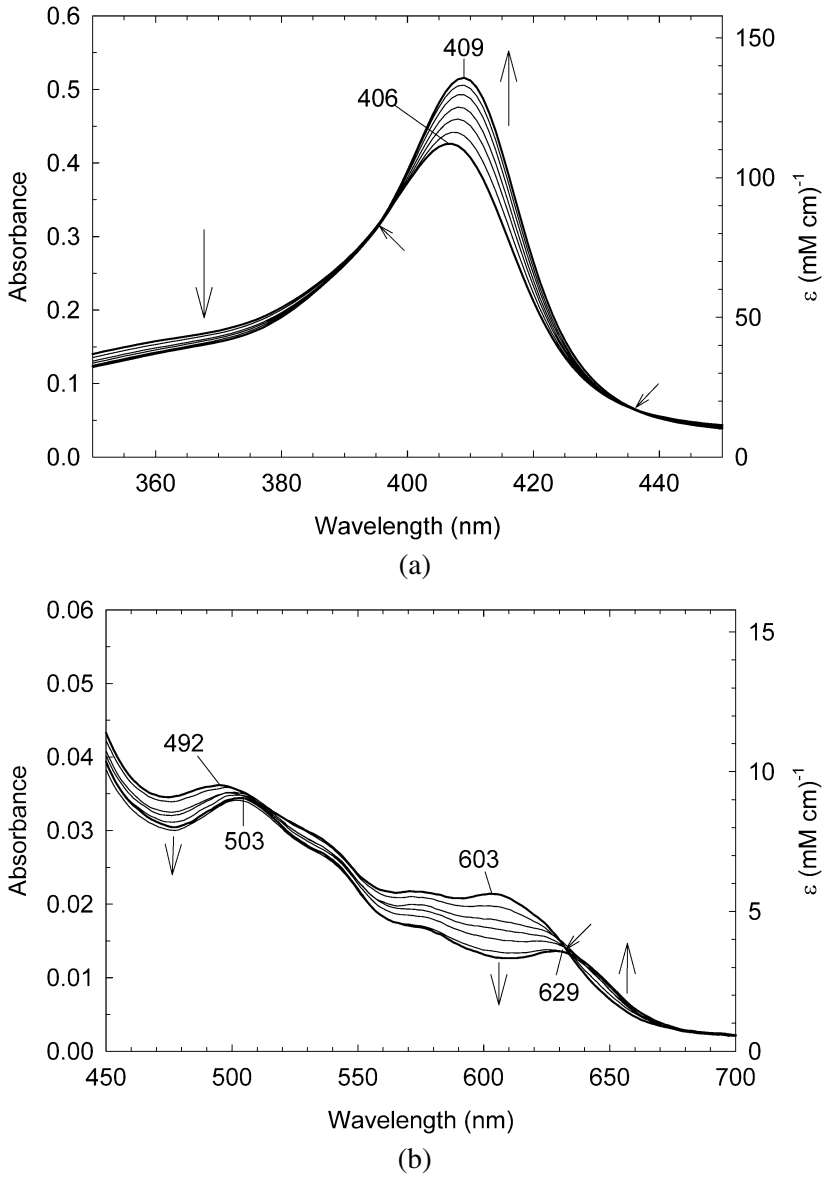

Fig. 1. (a) Soret region and (b) visible region EA spectral changes upon titration of exogenous ligand-free ferric H93G Mb (3.8 μM in a 1-cm cuvette) with low concentration (<100 μM) of imidazole (Im) in 0.1 M potassium phosphate buffer, pH 7.0, at 4°C. Vertical arrows indicate the directions of absorbance change on addition of 0, 2, 4, 8, 16, 32, 64 μM Im. The non-vertical short arrows show isosbestic points.

Soret absorption maximum (Fig. 1(a)). The resulting spectrum resembles that of the ferric wild-type Mb. These data indicate that a six-coordinate high-spin H93G Mb derivative with Im as a proximal ligand and water as a distal site ligand is generated. The ferric H93G (Im/water) Mb derivative at neutral pH is a heme iron coordination model for native Mb that cannot be prepared with simple synthetic heme iron model systems in organic solvents in the presence of Im. The crystal structure of Im-bound ferric H93G Mb, with Im in the proximal pocket, has been reported by Barrick [11] and is very similar to that of the ferric wild-type Mb.

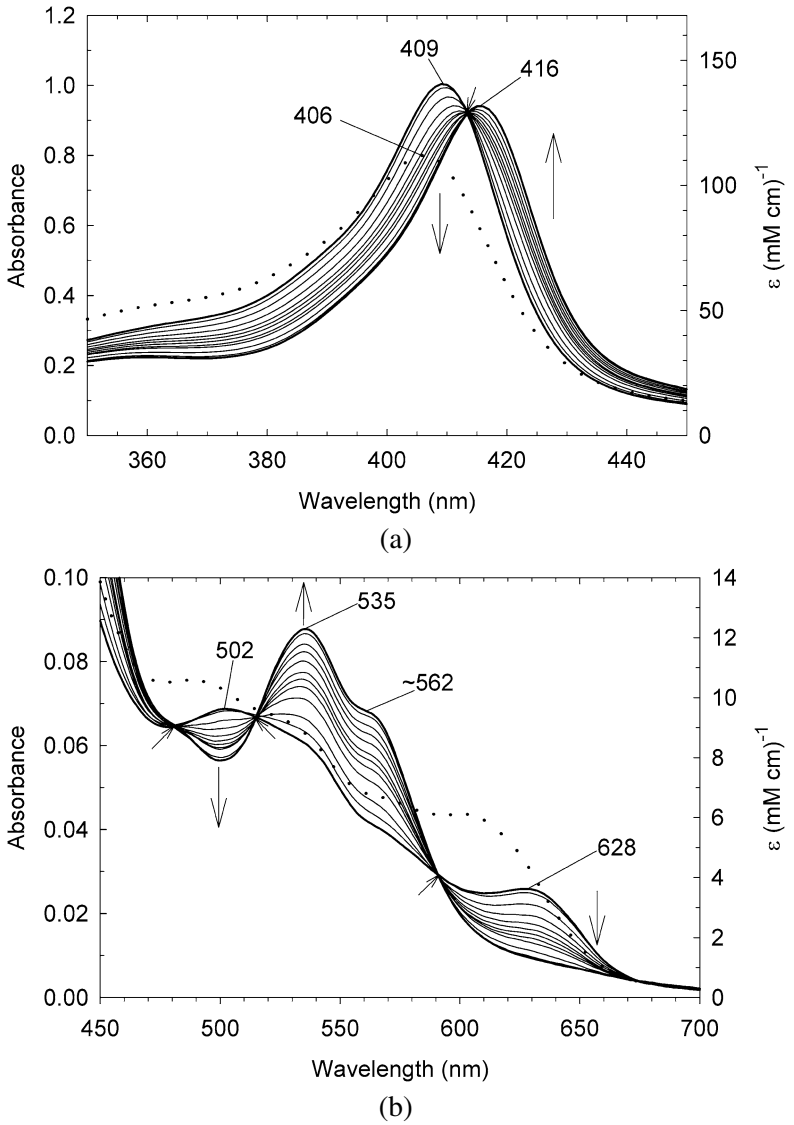

Fig. 2. (a) Soret region and (b) visible region EA spectral changes upon titration of exogenous ligand-free ferric H93G Mb (36 μM in a 0.2-cm cuvette) (dotted line) with high concentration (⩾0.5 mM) of imidazole (Im) in 0.1 M potassium phosphate buffer, pH 7.0, at 4°C. Vertical arrows indicate the directions of absorbance change on addition of 0.5, 1, 2, 3, 4, 5, 7, 10, 20, 50, 100 mM Im. The non-vertical short arrows show isosbestic points. The dotted lines are the EA spectrum of exogenous ligand-free ferric H93G Mb.

Upon millimolar addition of Im to ferric H93G(Im) Mb, the reaction enters the second phase process, i.e. second Im ligand binding to the heme center. The Soret absorption band is further red-shifted to 415 nm accompanied by a decrease in intensity (Fig. 2(a)). This leads to the formation of six-coordinate low-spin complex with EA and MCD spectral characteristics similar to those of the parallel wild-type Mb–Im complex in which distal water is replaced by Im (*vide infra*).

The isosbestic points observed in the Im titration data of either the first ligand binding to the proximal pocket or the second ligand binding to the distal pocket of H93G(Im) Mb support the use of a simple bimolecular association scheme to describe each of the two phases binding reaction (Eq. (5)). The bi-

molecular association scheme properly describes the binding reaction of Im to exogenous ligand-free ferric H93G Mb and to H93G(Im) Mb. The titration data have been analyzed by using a hyperbolic saturation plot (Fig. 3(a)) as well as Hill plot (Fig. 3(b)). The solid lines that have been drawn for the non-linear fit nicely fit with the data. The Hill plots in Fig. 3(b) yield a straight line with a slope of near unity ($n1 = 0.86$, $n2 = 1.06$), indicating that the ratio of ferric H93G Mb to Im and ferric H93G(Im) to Im is 1:1 (mol/mol). The dissociation constants ($K_{d1} = 6$ μM, $K_{d2} = 3.6$ mM) were calculated by the x axis intercept values ($= \log K_d$). The K_d value (6 μM) is similar to that (10 μM) reported by Roach et al. [21]. The 600-fold difference between the K_d values for the two phases demonstrates that the ligand binding affinity of the heme proximal site for the first ligand is much higher than that of the distal site for the second ligand.

Similar spectral changes are obtained upon the stepwise addition of Py (up to ∼50 mM) to exogenous ligand-free ferric H93G to generate the ferric H93G(Py) Mb complex (Fig. 4) having a Soret absorption peak at 408 nm. Hill plot analysis is shown as the inset of Fig. 4 with a slope of 0.87 and $K_d = 0.23$ mM. Upon further addition of higher concentrations of Py (>0.5 M), a secondary spectral change (decrease in the charge transfer bands at ∼500 and ∼600 nm and increase in absorbance between 520 and 580 nm) is observed that is indicative of second Py binding to mono-Py H93G Mb complex. In contrast to the Im binding case, the Soret absorption peak did not shift from 408 nm during the 2nd spectral change. However, further examination of the low-spin Py complex suggests that the heme is released from the protein environment to generate free heme-bis-Py complex in aqueous buffer judging from the complete absence of a CD signal for the complex. In fact, even the heme in wild-type Mb dissociates from the protein in the presence of 2 M Py at pH 7.0, 4°C to form a similar free heme-bis-Py complex (data not shown).

The dissociation constants determined in this work for the Im and Py complexes of ferric H93G Mb as well as a constant for the wild-type Mb–Im complex are summarized in Table 1. These K_d values are reproducible within ±10% ($K_d > 1$ mM) or ±20% ($K_d \leqslant 10$ μM). It is significant that the two sides of the heme in ferric H93G Mb behave differently when incorporating exogenous ligands. The proximal pocket has a much stronger binding affinity than the distal side judging by the absence of any evidence of mono-ligand binding to the distal pocket of H93G Mb [11] as well as by the quantitative measurements in this study. The ∼40-fold weaker affinity of the proximal site of the heme iron for Py ($K_{d1} = 0.23$ mM) than for Im ($K_{d1} = 6$ μM) may be due to the poorer σ-donor nature of the Py nitrogen ($pK_a = 5.3$) than that of Im nitrogen donor atom ($pK_a = 7.0$) [6]. Roach et al. [21] replaced the distal His with aspartate in the H64D/H93G Mb double mutant and found that Im binds to the heme iron to form only a bis-Im complex without intermediate formation of a mono-Im bound state. This result indicated that the distal pocket of the H64D/H93G Mb double mutant no longer has a weaker affinity for the second Im ligand binding to the heme iron. They attributed the result to a reduction of steric hindrance caused by the distal histidine in wild-type Mb which had been replaced by a smaller-sized side chain of aspartate in the double mutant. In fact, the crystal structure of ferric sperm whale Mb–Im complex reported by Lionetti et al. [22] clearly demonstrated a repulsive steric interaction between the heme-coordinated Im and the distal His. It is noted that the wild-type ferric Mb has ∼6-times lower affinity ($K_d = 22$ mM) than the H93G Mb mutant ($K_d = 3.6$ mM) for the second Im binding, presumably due to reduced steric hindrance by the distal His in the mutant. The structures of the Im-bound wild-type and mutant Mb may be somewhat different.

3.2. *EA spectra-monitored first and second ligand binding to the proximal and distal pockets of ferrous H93G Mb*

Like the case of ferric H93G Mb, titration data of Im to the dithionite-reduced deoxyferrous H93G Mb also produces changes in the EA spectrum with two sets of isosbestic points, suggesting that Im binding

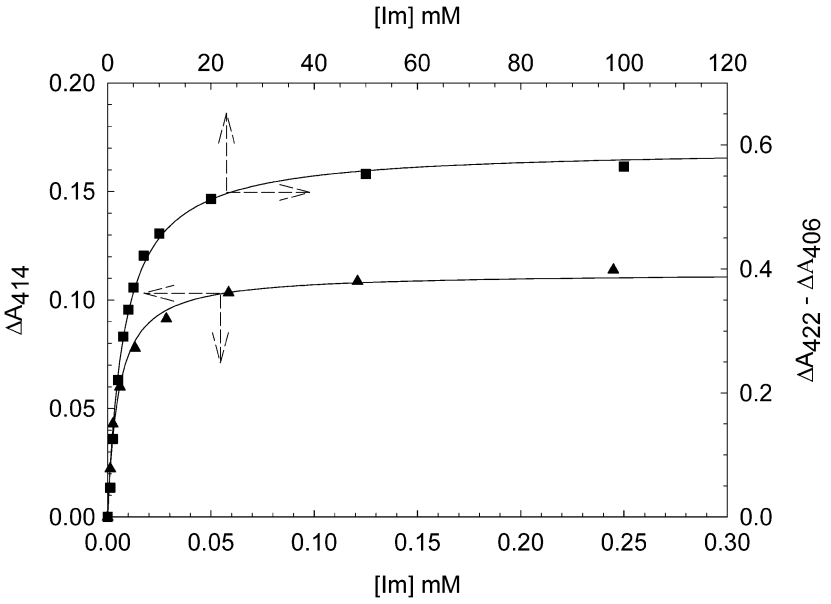

(a)

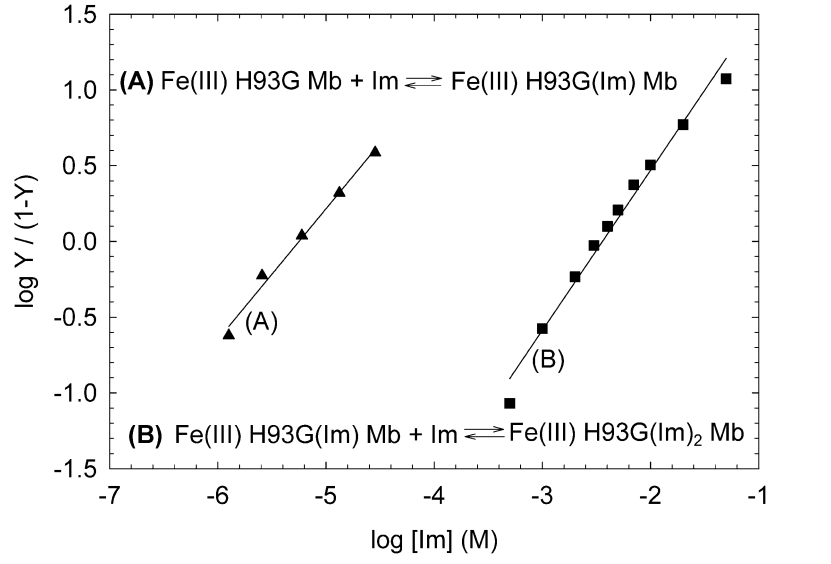

(b)

Fig. 3. (a) Hyperbolic saturation plots of the imidazole (Im) titration results shown in Fig. 1(a) (ligand-free) and Fig. 2(a) (mono-Im-bound) for Im binding to exogenous ligand-free (closed triangle) and mono-Im-bound (closed square) ferric H93G Mb. Maximum absorbance changes in difference spectra (not shown) ($\Delta A_{\lambda 1}$ or $\Delta A_{\lambda 1} - \Delta A_{\lambda 2}$, where $\lambda 1$ and $\lambda 2$ are wavelengths at which maximum positive (peak) and negative (trough) absorbance changes are observed, respectively) in the Soret region are plotted as a function of total ligand concentration. Lines drawn are non-linear fits for a bimolecular association model to the data using Eq. (5). (Closed triangle) First Im binding to H93G Mb and (closed square) second Im binding to H93G(Im) Mb data are plotted with different scales, left/bottom and right/top, respectively (see dashed arrows). (b) Hill plot of the titration data shown in (a). In the Y-axis label, Y is fractional saturation of H93G Mb with Im; thus, $Y/(1-Y) =$ [mono-Im-bound Mb]/[Im-free Mb] for (A) and [bis-Im-bound Mb]/[mono-Im-bound Mb] for (B). The Hill plots yield $K_{d1} = 6 \times 10^{-6}$ M (6.0 μM) (closed triangles) and $K_{d2} = 3.6 \times 10^{-3}$ M (3.6 mM) (closed squares) with slopes of 0.86 and 1.06, respectively.

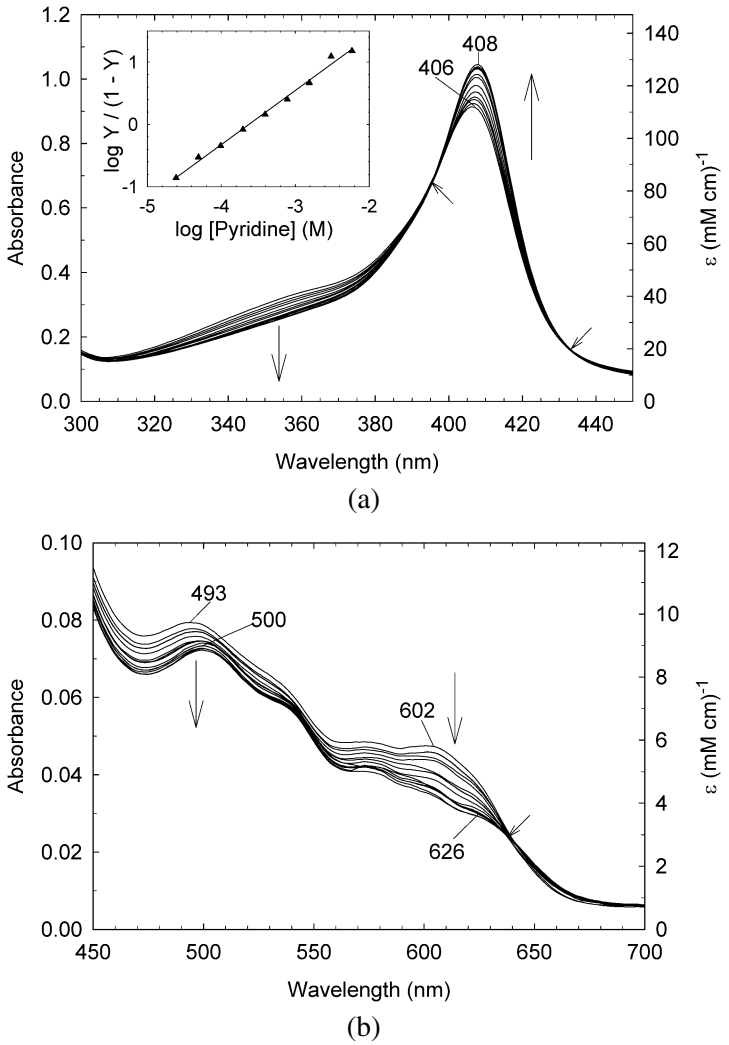

Fig. 4. (a) Soret region and (b) visible region EA spectral changes upon titration of exogenous ligand-free ferric H93G Mb (7.7 μM in a 1-cm cuvette) with pyridine (Py) in 0.1 M potassium phosphate buffer, pH 7.0, at 4°C. Vertical arrows indicate the directions of absorbance change on addition of 0, 0.025, 0.05, 0.1, 0.2, 0.4, 0.8, 1.5, 3.0, 6.0 mM Py. The short non-vertical arrows show isosbestic points. The Hill plot of the titration data is shown in the inset. In the Y-axis label, Y is the fractional saturation of H93G Mb with Py; thus, $Y/(1-Y) =$ [Py-bound Mb]/[Py-free Mb]. The Hill plots yields $K_{\rm d} = 2.3 \times 10^{-4}$ M (0.23 mM) with a slope of 0.87.

Table 1
Dissociation constant ($K_{\rm d}$) of ferric H93G Mb–ligand complexes[a]

Ligand (L)	p$K_{\rm a}$	Mono(L) complex	Bis(L_2) complex
		$K_{\rm d1}$	$K_{\rm d2}$
Imidazole	7.0	6 μM	3.6 mM
Pyridine	5.3	0.23 mM	–[b]
Imidazole (WT Mb)	7.0	–[c]	22 mM

[a]In 0.1 M potassium phosphate, pH 7.0, at 4°C. [b]Protein complex not formed (see text). [c]Not applicable.

is also a two-phase process. We found that ferrous H93G Mb, especially at low concentrations (<5 μM), was extremely sensitive to the presence of a small amount of O_2 prior to dithionite reduction and to introduction of O_2 upon addition of microliter aliquots of ligands to protein solutions in the presence of excess dithionite. Under such conditions, inconsistent absorption peak heights and spectral shapes of deoxyferrous H93G Mb were often observed. In addition, spectral changes during ligand titrations showed gradual deviation of isosbestic points and lack of saturation points. Fortunately, addition of micromolar bovine liver catalase to H93G Mb solutions prior to dithionite reduction eliminated such problems. This suggests that a small amount of hydrogen peroxide was generated when insufficiently anaerobic protein and ligand solutions were mixed with dithionite.

At micromolar Im concentrations, the Soret absorption band of ligand-free ferrous H93G Mb loses intensity and red-shifts from 428 nm to 430 nm (Fig. 5(a)), indicating the formation of mono-Im ferrous H93G Mb in which Im coordinates to the heme iron in the proximal pocket as demonstrated previously by Barrick [5,24]. In this study, we have further increased the concentration of Im in the protein solution to ∼40 mM and found that the second Im binding took place on the distal site of the heme (Fig. 6). During the second phase, there is an intensity increase and a blue-shift of the Soret EA maximum (Fig. 6(a)). Even though Im saturation is not reached even at the maximum concentration employed (1330 mM, pH 7.0) for the second Im binding, a saturation point (ΔA_{max}) has been determined by a hyperbolic saturation plot (Fig. 7(a)). Based on Hill plots, dissociation constants of 2 μM for the first and 610 mM for the second Im binding to deoxyH93G Mb at pH 7.0 and 4°C are obtained (Fig. 7(b)). In the ferrous state, the binding affinity of the first Im to the proximal pocket is about 3×10^5 times higher (i.e. lower K_d) than that of the second Im to the distal site.

Pyridine titration of exogenous ligand-free deoxyferrous H93G Mb has also been carried out (Figs 5(b) and 8). Similar to the Im titration results, there are two sets of isosbestic points, but the spectral changes are not exactly the same as those observed for the corresponding Im titration. The Soret absorption peak blue-shifts and the peak intensity decreases during the first ligand binding phase (Fig. 5(b)) and then further blue-shifts and increases during the second phase (Fig. 8(a)). Dissociation constants calculated by Hill plot (Fig. 9(b)) are $K_{d1} = 10$ μM and $K_{d2} = 2.4$ mM. There is a 240-fold difference between the affinity of the first and of second Py binding to the proximal and distal pocket, respectively.

The titration results (K_d values) for the Im and Py binding to ferrous H93G Mb are summarized in Table 2, which includes an estimated K_d value (∼8 M) of the wild-type ferrous Mb–Im complex. Under the same conditions, a K_d value for the wild-type ferrous Mb–Py complex was ∼0.1 M (this study). As is the case of ferric H93G Mb, the distal pocket of wild-type ferrous Mb has much lower affinity for Im (by about thirteen-fold) than the mutant. Furthermore, in contrast to the results of ferric H93G Mb (Table 1), Im and Py have relatively similar affinities ($K_{d1} = 2$ and 10 μM, respectively) for the proximal pocket of ferrous H93G Mb. However, the Py affinity ($K_{d2} = 2.4$ mM) for the distal site of the heme iron in ferrous H93G Mb is much (by ∼250 fold) higher than that for Im ($K_{d2} = 610$ mM). The same trend is observed for Im and Py binding to ferrous wild-type Mb. This is likely to be attributed to the better π-acceptor property of Py than Im [6].

3.3. MCD and EA spectroscopic investigation of mono- and bis-ligated H93G Mb compounds

In earlier studies, our lab has examined ferric/ferrous H93G(Im) Mb and ferric H93G(bis-Im) Mb with MCD spectroscopy [13]. Here, we investigate ferric mono-Py and ferrous mono-/bis-Py H93G Mb and ferrous H93G(bis-Im) Mb complexes that have not been previously characterized with MCD spectroscopy. Figure 10 compares the MCD and EA spectra of ferric H93G(Py) Mb and ferric H93G(Im)

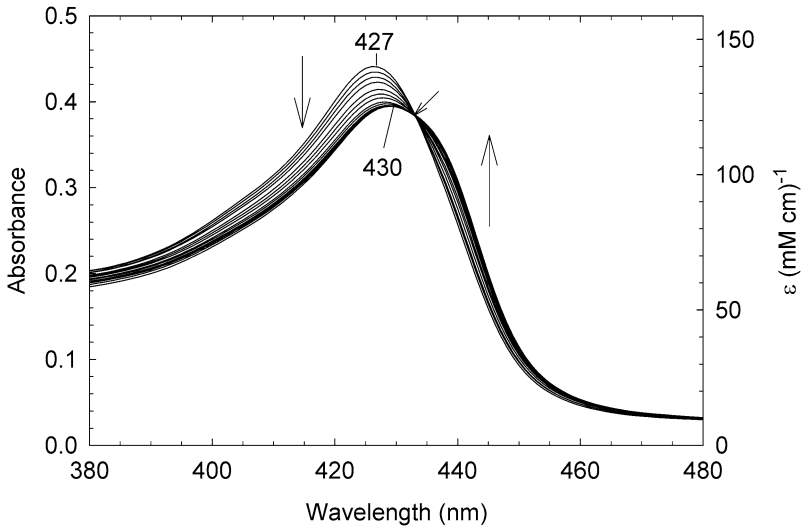

(a)

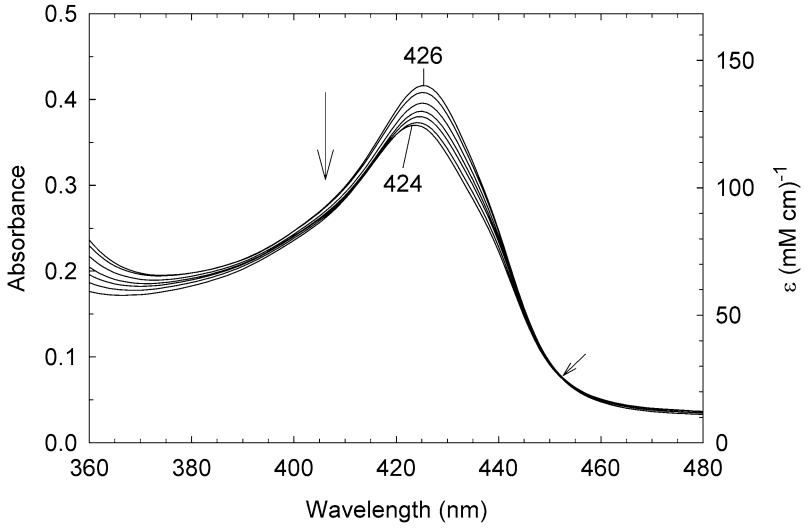

(b)

Fig. 5. (a) Soret region EA spectral changes upon titration of exogenous ligand-free ferrous H93G Mb (3.4 μM in a 1-cm cuvette) with low concentration (<150 μM) of imidazole (Im) in 0.1 M potassium phosphate buffer, pH 7.0, at 4°C. The titration was performed in the presence of 0.5 μM (based on heme) catalase (see text). Vertical arrows indicate the directions of absorbance change on addition of 0, 1, 2, 4, 8, 16, 32, 63, 127 μM Im. The short non-vertical arrows show isosbestic points. (b) Soret region electronic absorption (EA) spectral changes upon titration of exogenous ligand-free ferrous H93G Mb (3.5 μM in a 1-cm cuvette) with low concentration (<100 μM) of pyridine (Py) in 0.1 M potassium phosphate buffer, pH 7.0, at 4°C. Vertical arrows indicate the directions of absorbance change on addition of 0, 2.5, 5, 10, 20, 40, 80 μM Py. The short non-vertical arrows show isosbestic points.

Mb. The band patterns of MCD and EA spectra of ferric H93G(Py) Mb are quite similar to those of the ferric H93G(Im) Mb, indicating that the electronic structures and thus the heme iron-ligand coordination modes of the two protein derivatives are comparable.

Figure 11 compares the MCD and EA spectra of ferric H93G Mb in the presence of 4 M Im and 2 M

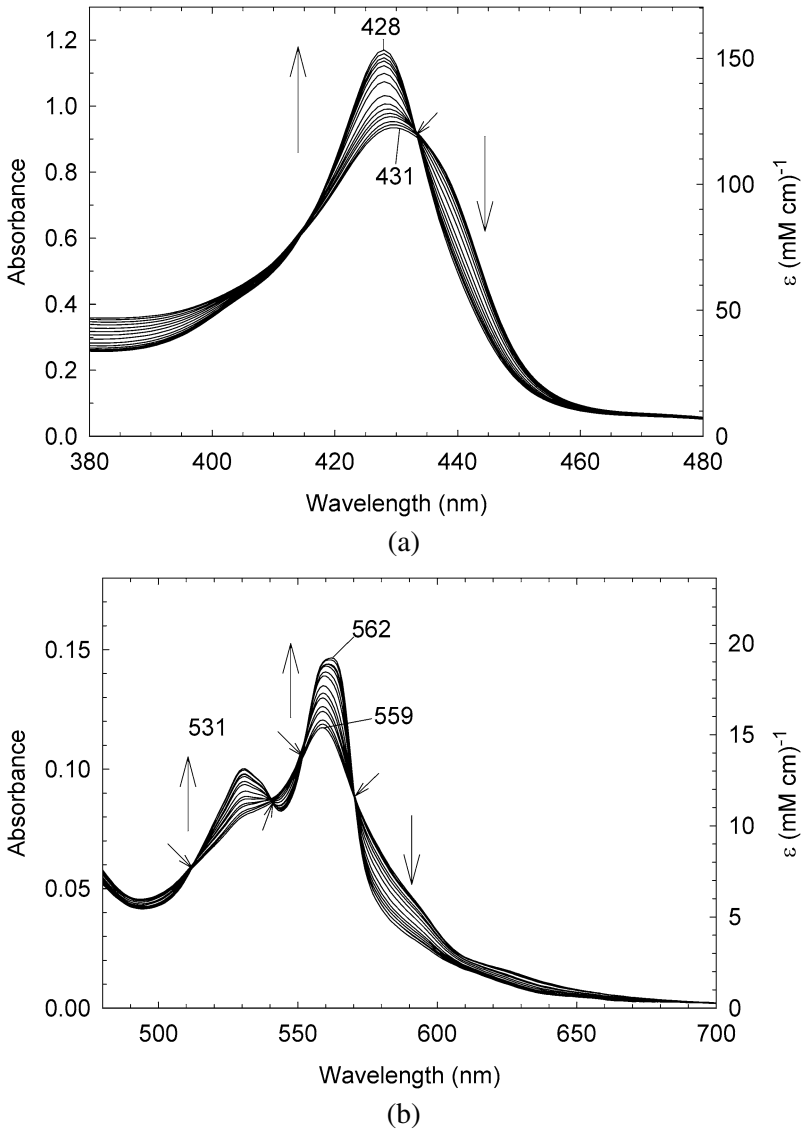

Fig. 6. (a) Soret region and (b) visible region EA spectral changes upon titration of exogenous ligand-free ferrous H93G Mb (38 μM in a 0.2-cm cuvette) with high concentration (>30 mM) of imidazole (Im) in 0.1 M potassium phosphate buffer, pH 7.0, at 4°C. Vertical arrows indicate the directions of absorbance change on addition of 36, 72, 140, 270, 500, 710, 890, 1050, 1200, 1330 mM Im. The non-vertical short arrows show isosbestic points.

Py and wild-type Mb in the presence of 1 M Im, all recorded at pH 7.0 at 4°C. Even though the Py complex appears to be protein-free (*vide supra*), its spectra are included in Fig. 11 for comparison. The ferric bis-Im H93G Mb as well as bis-Py heme complexes are clearly six-coordinate low-spin complexes and, as such, are very similar to those of the wild-type Mb coordinated by Im in the distal side as well as ferric cytochrome b_5 (spectra not shown), a native bis-His ligated heme protein, except for some (5–10 nm) blue-shifts for the bis-Py complex.

Reduction of ferric H93G(Im) Mb (2 mM Im) with sodium dithionite results in formation of a five-

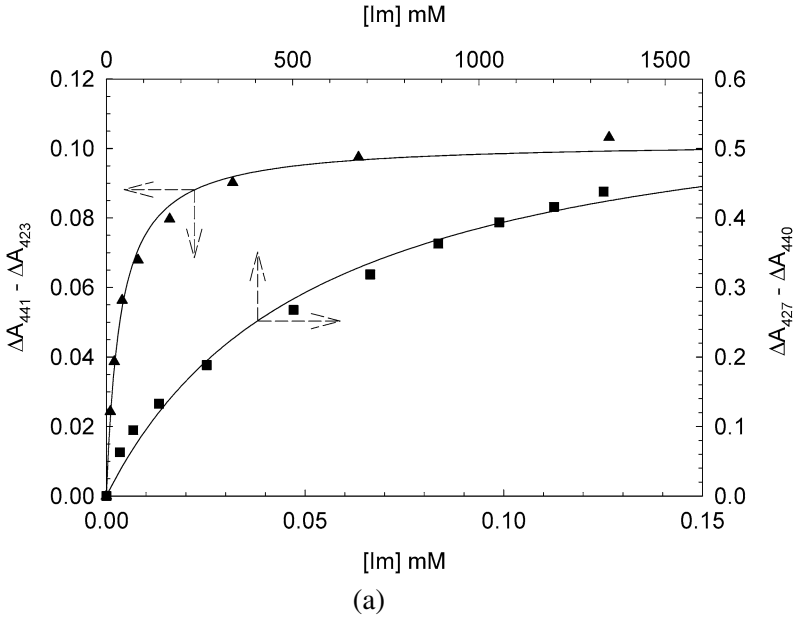

(a)

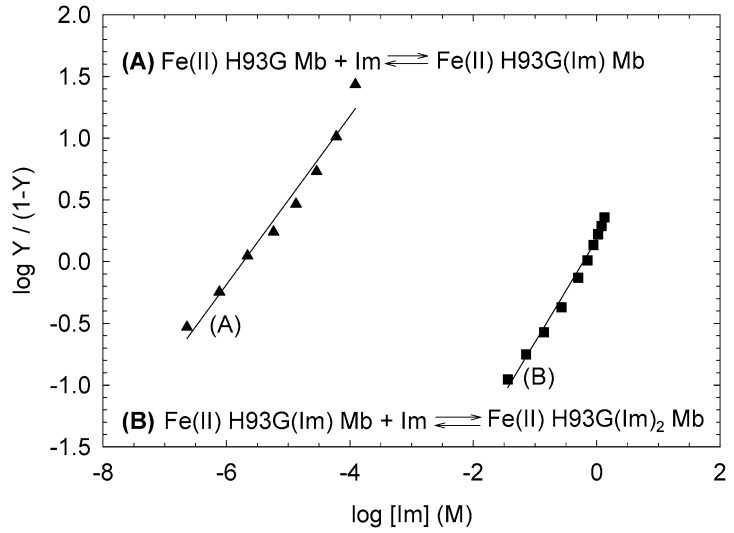

(b)

Fig. 7. (a) Hyperbolic saturation plots of the imidazole (Im) titration results shown in Fig. 5(a) (ligand-free) and Fig. 6(a) (mono-Im-bound) for Im binding to exogenous ligand-free (closed triangle) and mono-Im-bound (closed square) ferrous H93G Mb. Initial 3 data points in the titration (Fig. 5(a)) that gave less than 10% saturation were excluded from the hyperbolic plot and Hill plot, because the spectra changes were too small to gave accurate data plot. Maximum absorbance changes in difference spectra in the Soret region are plotted as a function of total ligand concentration. Lines drawn are non-linear fits for a bimolecular association model to the data using Eq. (5). First Im binding to H93G Mb (closed triangle) and second Im binding to H93G(Im) Mb (closed square) data are plotted with different scales, left/bottom and right/top, respectively (see dashed arrows). (b) Hill plot of the titration data shown in (a). In the Y-axis label, Y is fractional saturation of H93G Mb with Im; thus, $Y/(1-Y) =$ [mono-Im-bound Mb]/[Im-free Mb] for (A) and [bis-Im-bound Mb]/[mono-Im-bound Mb] for (B). The Hill plots yield $K_{d1} = 2 \times 10^{-6}$ M (2 μM) (closed triangles) and $K_{d2} = 6.1 \times 10^{-1}$ M (0.61 M) (closed squares) with slopes of 0.68 and 0.83, respectively.

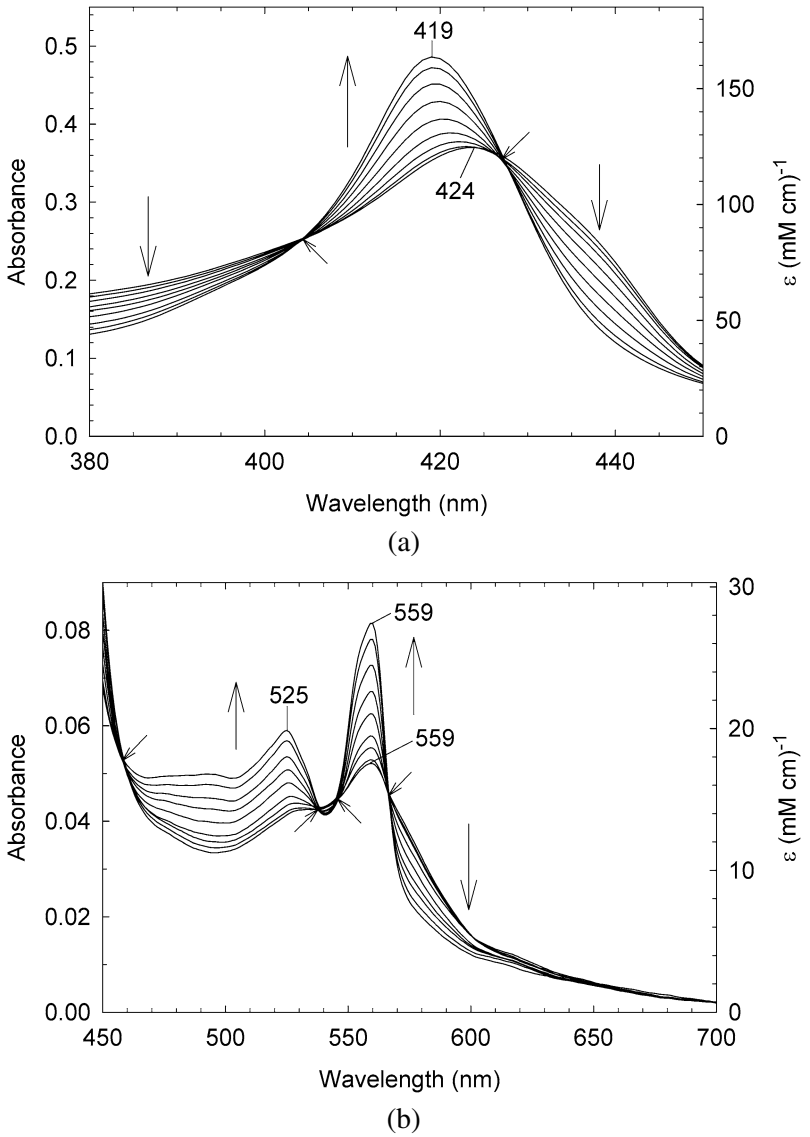

Fig. 8. (a) Soret region and (b) visible region EA spectral changes upon titration of exogenous ligand-free ferrous H93G Mb (3.5 μM in a 1-cm cuvette) with high concentration (>0.15 mM) of pyridine (Py) in 0.1 M potassium phosphate buffer, pH 7.0, at 4°C. Vertical arrows indicate the directions of absorbance change on addition of 0.16, 0.32, 0.63, 1.2, 2.4, 4.8, 8.5, 18.1 mM Py. The non-vertical arrows show isosbestic points.

coordinate high-spin complex with EA and MCD spectral characteristics very similar to those of deoxy-ferrous wild-type Mb (Fig. 12). Furthermore, bis-Py and bis-Im ferrous H93G Mb complexes can be generated in the presence of higher concentrations of Py (∼33 mM, pH 7) and Im (4 M, pH 7), respectively. In molar concentration of Py, however, ferrous H93G Mb formed a protein-free (no CD signal) low spin complex whose MCD and EA spectra (not shown) are similar in overall feature, but distinct in detail from those of the ferrous bis-Py H93G Mb. The MCD spectral pattern of ferrous H93G (bis-Im) Mb is not exactly identical to that of ferrous H93G (bis-Py) Mb whose MCD spectral pattern is similar to that of ferrous cytochrome b_5 [25], especially in the Soret region (Fig. 13). We estimate the saturation

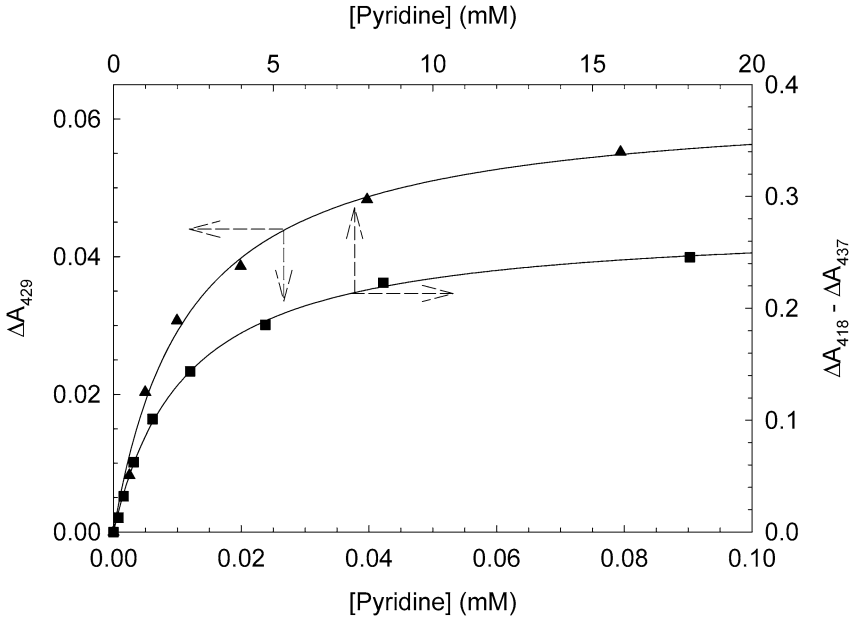

(a)

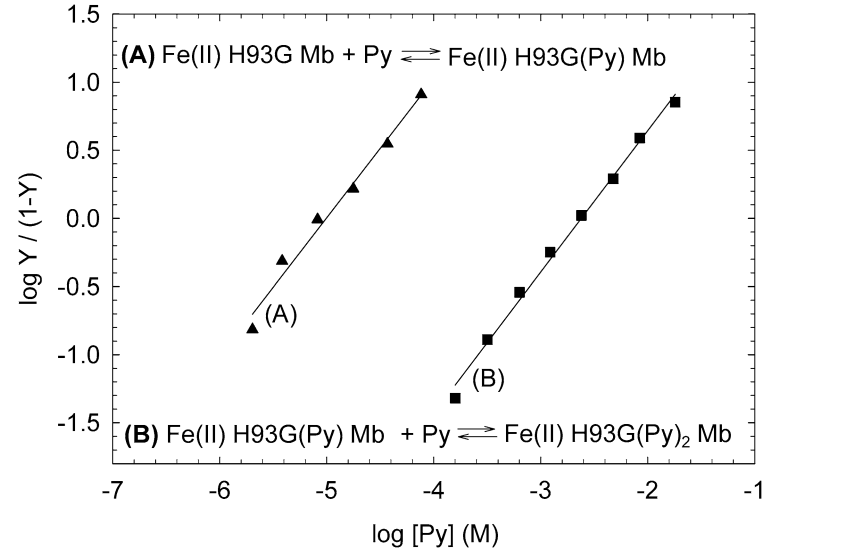

(b)

Fig. 9. (a) Hyperbolic saturation plots of the pyridine (Py) titration results shown in Fig. 5(b) (ligand-free) and Fig. 8(a) (mono-Py-bound) for Py binding to exogenous ligand-free (closed triangle) and mono-Py-bound (closed square) ferrous H93G Mb. Maximum absorbance changes in difference spectra (not shown) in the Soret region are plotted as a function of total ligand concentration. Lines drawn are non-linear fits for a bimolecular association model to the data using Eq. (5). First Py binding to H93G Mb (closed triangle) and second Py binding to H93G(Py) Mb (closed square) data are plotted with different scales, left/bottom and right/top, respectively (see dashed arrows). (b) Hill plots of the titration data shown in (a). In the Y-axis label, Y is fractional saturation of H93G Mb with Py; thus, $Y/(1-Y) =$ [mono-Py-bound Mb]/[Py-free Mb] for (A) and [bis-Py-bound Mb]/[mono-Py-bound Mb] for (B). The Hill plots yield $K_{d1} = 1 \times 10^{-5}$ M (10 μM) (closed triangles) and $K_{d2} = 2.4 \times 10^{-3}$ M (2.4 mM) (closed squares) with slopes of 1.02 and 1.04, respectively.

Table 2
Dissociation constant (K_d) of ferrous H93G Mb–ligand complexes[a]

Ligand (L)	pK_a	Mono(L) complex	Bis(L_2) complex
		K_{d1}	K_{d2}
Imidazole	7.0	2 μM	610 mM
Pyridine	5.3	10 μM	2.4 mM
Imidazole (WT Mb)	7.0	–[b]	∼8 M[c]

[a]In 0.1 M potassium phosphate, pH 7.0, at 4°C. [b]Not applicable. [c]Estimated based on ∼33% saturation with 4 M Im (this study).

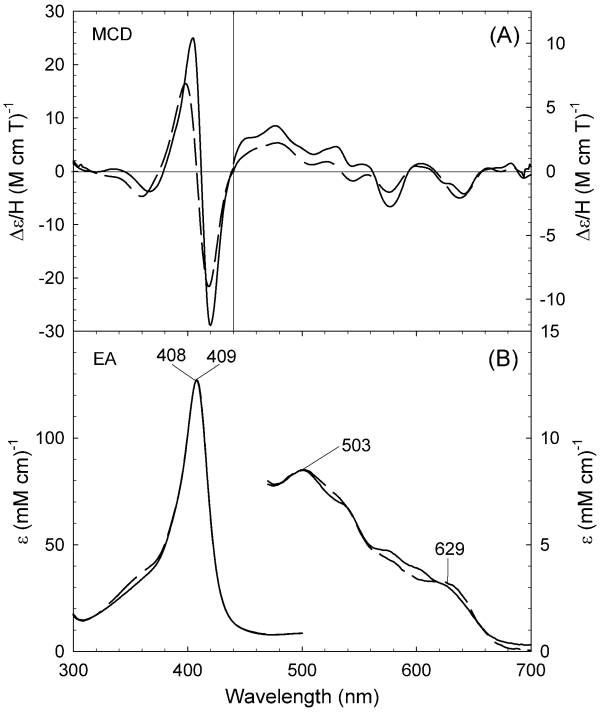

Fig. 10. (A) MCD and (B) EA spectra of ferric H93G(Py) Mb (solid line, 33 mM Py), ferric H93G (Im) Mb (dashed line, 1 mM Im) and ferric wild-type Mb (dotted line) in 0.1 M potassium phosphate buffer, pH 7.0, at 4°C. The spectra for ferric H93G(Im) Mb are replotted from [23].

(Y) of bis-Im H93G Mb complex with Im is ∼87% based on the K_d value (610 mM) and Im concentration (4 M) used to generate the complex ($Y = 4/4.61 = 0.87$). Perhaps the incomplete Im saturation in ferrous H93G (bis–Im) Mb may be a cause of its MCD spectral deviation from the spectrum of ferrous cytochrome b_5.

4. Conclusions

In summary, this study reports a thorough comparison of the dissociation constants for Im and Py binding to the proximal and distal sites of the heme iron, respectively, to form mono- and bis-ligated complexes in both the ferric and ferrous H93G Mb cavity mutant. The ligand binding affinities for

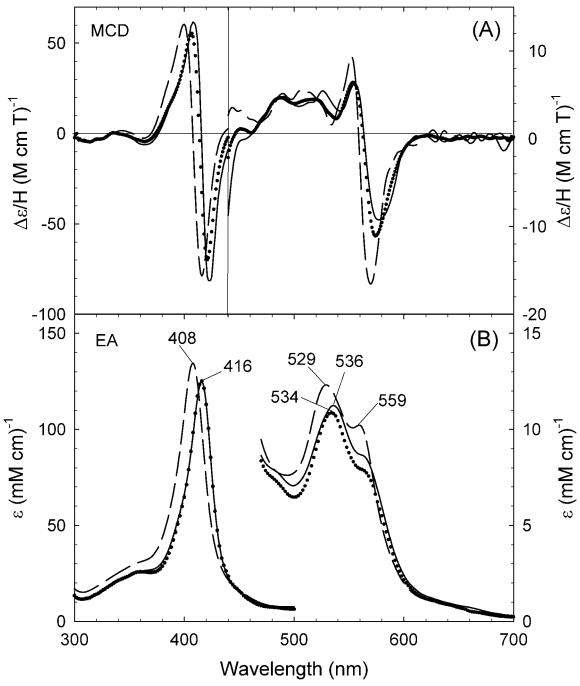

Fig. 11. (A) MCD and (B) EA spectra of ferric H93G (bis-Im) Mb (solid line, 4 M Im) and ferric wild-type Mb(Im) (dotted line, 1 M Im) in 0.1 M potassium phosphate buffer, pH 7.0, at 4°C. Spectra of protein-free ferric bis-Py heme complex (dashed line) that was generated by adding 2 M Py to exogenous ligand-free H93G are also plotted for comparison (see text).

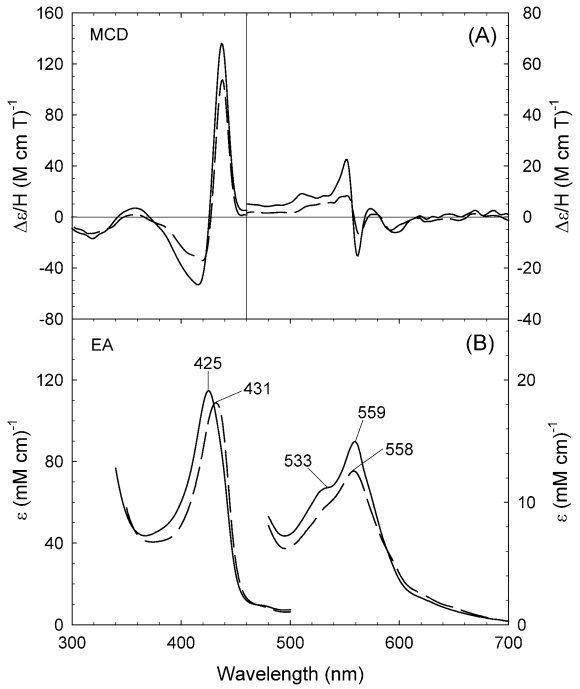

Fig. 12. (A) MCD and (B) EA absorption spectra of ferrous H93G(Py) Mb (solid line, 100 μM Py) and H93G (Im) Mb (dashed line, 2 mM Im) in 0.1 M potassium phosphate buffer, pH 7.0, at 4°C.

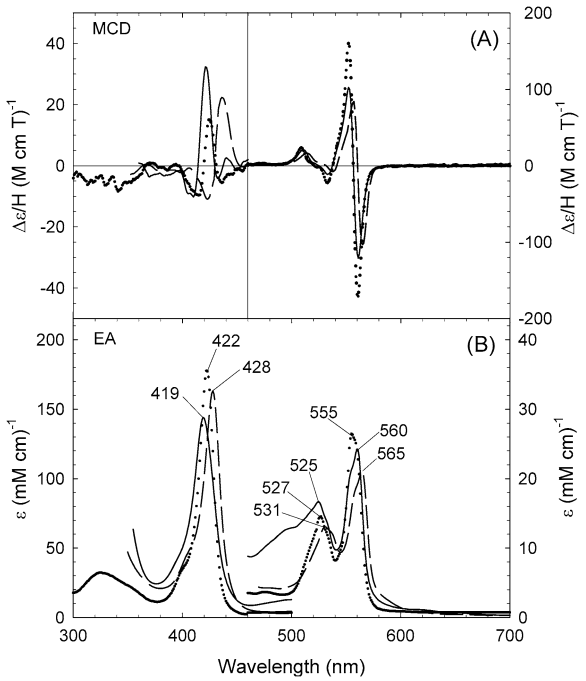

Fig. 13. (A) MCD and (B) EA absorption spectra of ferrous H93G (bis-Py) Mb (solid line, 33 mM Py), ferrous H93G(bis-Im) Mb (dashed line, 4 M Im) and ferrous cytochrome b_5 (dotted line) in 0.1 M potassium phosphate buffer, pH 7.0, at 4°C. The spectra for ferric cytochrome b_5 are replotted from [25].

these two sides are one hundred- to one thousand-fold different. It is apparent that the proximal pocket of H93G Mb is the much preferred binding site for exogenous ligands. At higher concentrations of ligand (>1 mM), it is possible to overcome the steric hindrance of the distal site (likely due to the distal His64) and form bis-ligand complexes. To our knowledge, this is the first time that Py-bound equilibrium constants and spectroscopic properties of H93G Mb have been examined in ferric (except for tabulated EA peak positions [26]) as well as ferrous states. The spectra observed for the Py-bound H93G Mb are similar to that of the parallel Im-bound H93G Mb and wild-type Mb or cytochrome b_5. This study provides quantitative evidence for the differential ligand binding affinities of the proximal and distal pockets of the H93G Mb cavity mutant, a unique property that facilitates the generation of several heme iron derivatives not easily prepared with other heme model systems. The present work also lays the foundation for future studies of H93G Mb with less common ligands such as amines, thioether or other neutral and anionic non-nitrogen donor ligands.

Acknowledgment

We thank Professor Steven G. Boxer for the H93G expression system and Drs. Alycen Pond Nigro, Roshan Perera and Mark Roach for helpful discussions. Financial support is acknowledged from the NIH (GM 26730 to J.H.D.).

References

[1] J.H. Dawson, Probing structure-function relations in heme-containing oxygenases and peroxidases, *Science* **240** (1988), 433–439.

[2] C.K. Chang and T.G. Traylor, Synthesis of myoglobin active-site, *Proc. Natl. Acad. Sci. USA* **70** (1973), 2647–2650.
[3] J.P. Collman, Synthetic models for oxygen-binding hemeproteins, *Acc. Chem. Res.* **10** (1977), 265–272.
[4] G.E. Wuenschell, C. Tetreau, D. Lavalette and C.A. Reed, H-bonded oxyhemoglobin models with substituted picket-fence porphyrins: The model compound equivalent of site-directed mutagenesis, *J. Am. Chem. Soc.* **114** (1992), 3346–3355.
[5] T.G. Traylor, Synthetic model compounds for heme proteins, *Acc. Chem. Res.* **14** (1981), 102–109.
[6] H.M. Marques, Insights into porphyrin chemistry provided by the microperoxidases, the haempeptides derived from cytochrome c, *Dalton Trans.* **39** (2007), 4371–4385.
[7] E. Antonini and M. Brunori, *Hemoglobin and Myoglobin in Their Reactions with Ligands*, North-Holland Publishing Co., Amsterdam, 1971.
[8] C.L. Coyle, P.A. Rafson and E.H. Abbott, Equilibriums of imidazole with iron(III) tetraphenylporphine, *Inorg. Chem.* **12** (1972), 2007–2010.
[9] F.A. Walker, M.-W. Lo and M.T. Ree, Electronic effects in transition metal porphyrins. The reactions of imidazoles and pyridines with a series of para-substituted tetraphenylporphyrin complexes of chloroiron(III), *J. Am. Chem. Soc.* **98** (1976), 5552–5560.
[10] D. Brault and M. Rougee, Ferrous porphyrins in organic solvents. I. Preparation and coordinating properties, *Biochemistry* **13** (1974), 4591–4597.
[11] D. Barrick, Replacement of the proximal ligand of sperm whale myoglobin with free imidazole in the mutant His-93 → Gly, *Biochemistry* **33** (1994), 6546–6554.
[12] R. Perera and J.H. Dawson, Modeling heme protein active sites with the his93gly cavity mutant of sperm whale myoglobin: complexes with nitrogen-, oxygen- and sulfur-donor proximal ligands, *J. Porphyrins Phthalocyanines* **8** (2004), 246–254.
[13] A.E. Pond, M.P. Roach, M.R. Thomas, S.G. Boxer and J.H. Dawson, The H93G myoglobin cavity mutant as a versatile template for modeling heme proteins: ferrous, ferric, and ferryl mixed-ligand complexes with imidazole in the cavity, *Inorg. Chem.* **39** (2000), 6061–6066.
[14] M.P. Roach, A.E. Pond, M.R. Thomas, S.G. Boxer and J.H. Dawson, The role of the distal and proximal protein environments in controlling the ferric spin state and in stabilizing thiolate ligation in heme systems: thiolate adducts of the myoglobin H93G cavity mutant, *J. Am. Chem. Soc.* **121** (1999), 12088–12093.
[15] J.H. Dawson, A.E. Pond and M.P. Roach, H93G myoglobin cavity mutant as versatile template for modeling heme proteins: Magnetic circular dichroism studies of thiolate- and imidazole-ligated complexes, *Biopolymers (Biospectroscopy)* **67** (2002), 200–206.
[16] R. Perera, M. Sono, J.A. Sigman, T.D. Pfister, Y. Lu and J.H. Dawson, Neutral thiol as a proximal ligand to ferrous heme iron: Implications for heme proteins that lose cysteine thiolate ligation on reduction, *Proc. Natl. Acad. Sci. USA* **100** (2003), 3641–3646.
[17] J. Cheek and J.H. Dawson, Magnetic circular dichroism spectroscopy of heme iron systems, in: *The Porphyrin Handbook*, K. Kadish, K. Smith and R. Guilard, eds, Academic Press, New York, 2000, pp. 339–369.
[18] A.E. Pond, M.P. Roach, M. Sono, A.H. Rux, S. Franzen, R. Hu, M.R. Thomas, A. Wilks, Y. Dou, M. Ikeda-Saito, P.R. Ortiz de Montellano, W.H. Woodruff, S.G. Boxer and J.H. Dawson, Assignment of the heme axial ligand(s) for the ferric myoglobin (H93G) and heme oxygenase (H25A) cavity mutants as oxygen donors using magnetic circular dichroism, *Biochemistry* **38** (1999), 7601–7608.
[19] K.-G. Paul, H. Theorell and Å. Åkeson, The molar light absorption of pyridine ferroprotoporphyrin (pyridine haemochromogen), *Acta Chem. Scand.* **7** (1953), 1284–1287.
[20] A.M. Huff, C.K. Chang, D.K. Cooper, K.M. Smith and J.H. Dawson, Imidazole- and alkylamine-ligated iron(II,III) chlorin complexes as models for histidine and lysine coordination to iron in dihydroporphyrin-containing proteins: characterization with magnetic circular dichroism spectroscopy, *Inorg. Chem.* **32** (1993), 1460–1466.
[21] M.P. Roach, S. Ozaki and Y. Watanabe, Investigations of the myoglobin cavity mutant H93G with unnatural imidazole proximal ligands as a modular peroxide O–O bond cleavage model system, *Biochemistry* **39** (2000), 1446–1454.
[22] C. Lionetti, M.G. Guanziroli, F. Frigerio, P. Ascenzi and M. Bolognesi, X-ray crystal structure of the ferric sperm whale myoglobin: imidazole complex at 2.0 A resolution, *J. Mol. Biol.* **217** (1991), 409–412.
[23] A.E. Pond, The H93G myoglobin cavity mutant as a spectroscopic model for heme proteins: a magnetic circular dichroism investigation of the ferrous, ferric and ferryl mixed ligand complexes with exogenous imidazole in the cavity, PhD dissertation, University of South Carolina, 1999.
[24] D. Barrick, Trans-substitution of the proximal hydrogen bond in myoglobin: II. Energetics, functional consequences, and implications for hemoglobin allostery, *Proteins* **39** (2000), 278–290.
[25] J. Cheek, D. Mandelman, T.L. Poulos and J.H. Dawson, A study of the K(+)-site mutant of ascorbate peroxidase: mutations of protein residues on the proximal side of the heme cause changes in iron ligation on the distal side, *J. Biol. Inorg. Chem.* **4** (1999), 64–72.
[26] G.D. DePillis, S.M. Decatur, D. Barrick and S.G. Boxer, Functional cavities in proteins: A general method for proximal ligand substitution in myoglobin, *J. Am. Chem. Soc.* **116** (1994), 6981–6982.